

**Mechanistic Insights into the Pore Confinement Effect on  
Bimolecular and Monomolecular Cracking Mechanisms of  
N-octane over HY and HZSM-5 Zeolites: A DFT Study**

Jia Fu, Xiang Feng, Yibin Liu, Honghong Shan, Chaohe Yang\*

*State Key Laboratory of Heavy Oil Processing, China University of Petroleum, Qingdao 266580,  
China*

Corresponding author: Chaohe Yang

E-mail: yangch@upc.edu.cn

Tel.: +86-0532-86981718

## **Abstract**

Bimolecular and monomolecular cracking mechanisms of alkanes simultaneously occur and have a competitive relationship, which strongly influences product distribution. In this work, the density functional theory (DFT) is firstly carried out to elucidate two cracking mechanisms in HZSM-5 and HY zeolites. It is found that the overall apparent reaction barrier for the monomolecular cracking reaction at 750 K in the HZSM-5 zeolite is 5.30 kcal/mol, much lower than that (23.12 kcal/mol) for bimolecular cracking reaction, indicating that monomolecular mechanism is predominant in the HZSM-5 zeolite. In contrast, the bimolecular mechanism is predominant in the HY zeolite due to lower apparent reaction barrier energy barrier (6.95 kcal/mol) for bimolecular cracking reaction than that (24.34 kcal/mol) for the monomolecular cracking reaction. Moreover, the intrinsic reason for the different mechanisms is further elucidated. The confinement effect can effectively decrease energy barrier when the size of transition state is comparable to pore-size of zeolite. The insights in this work will be of great significance to the understanding of confinement on catalytic cracking mechanism and to the design of highly efficient cracking catalysts.

## 1. Introduction

The fluid catalytic cracking (FCC) of hydrocarbons is one of the most important processes in the oil refining industry<sup>1,2</sup>. In the FCC process, alkane cracking is one of dominating reactions<sup>3</sup>. The catalytic cracking of alkanes is proposed to occur inevitably via bimolecular and monomolecular mechanisms<sup>4</sup>. Both mechanisms occur simultaneously and have a competitive relationship. The yield of products depends on which one of them is predominant in zeolites. If the monomolecular mechanism is dominant, the yield of light olefins (e.g. ethylene and propylene) will increase<sup>5</sup>. On the contrary, if the bimolecular cracking is dominant, the primary product will contain a large number of iso-paraffins and iso-olefins<sup>6</sup>. N-octane is a typical alkane for two cracking mechanisms and has appropriate number of carbon atoms. Therefore, mechanistic investigation on n-octane catalytic cracking is of prime scientific and industrial importance.

To date, the comparison of both reaction pathways were mainly speculated based on experimental data. The relative contribution of the two cracking mechanisms is expressed by the "cracking mechanism ratio" (CMR) as " $(C_1+C_2)/i-C_4$ " that is directly proportional to the ratio of monomolecular to bimolecular mechanism<sup>7,8</sup>. Corma et al.<sup>9</sup> found that the ratio of monomolecular to bimolecular cracking reaction increased with higher temperature and smaller pore-size of zeolites. However, catalytic cracking of n-alkane is a very complicated process and it is difficult to map out the detailed reaction mechanism solely by experimental methods<sup>10</sup>. What's more, experimental data usually

shows a qualitative result but not offers the interpretation for the origin of the catalytic reaction. Therefore, it is of great value to study the intrinsic catalytic cracking mechanism using theoretical calculation. The theoretical density function theory (DFT) calculation is a powerful approach to investigate the mechanisms of n-octane cracking. It can offer an atomic-level description of the complete reaction mechanism, including structures of reactant and transition state<sup>11, 12</sup>.

The intermediates and transition states are stabilized by the interaction with the acid site and the surrounding framework<sup>13-17</sup>. It is reported that zeolites with different framework can exhibit similar acid strengths<sup>13</sup>. Therefore, the reactivity can be greatly affected by the framework structure, which has an influence on the transition states of rate determining step, and then are responsible for the distinct products selectivities<sup>18</sup>.<sup>19</sup> ZSM-5 zeolite and Y zeolite have been widely applied to industrial catalytic cracking processes due to their high activities and selectivities<sup>20, 21</sup>. They usually have diverse influences on the reactivity of transition states due to their different pore shapes<sup>22, 23</sup>. HY zeolite has 12-membered ring connected supercages of  $7.4 \times 7.4 \text{ \AA}$ <sup>24</sup>, while HZSM-5 zeolite has 10-membered ring straight and zigzag pore channels of  $5.3 \times 5.6$  and  $5.1 \times 5.5 \text{ \AA}$ <sup>25</sup>. Iglesia et al.<sup>14</sup> reported that this different pore structure could change the activation barriers of  $C_3H_8$  cracking. Louis et al.<sup>19</sup> published that variation of the pore-shape at the critical transition states could lead to barrier height shifts on the order of 2.4-4.8 kcal/mol when they researched the m-xylene disproportionation in MFI, FAU and MOR zeolites. However, the effect of pore structure on the bimolecular and

monomolecular mechanisms of n-octane catalytic cracking in the HY and HZSM-5 zeolites were rarely studied in literature. Therefore, there is urgent need to understand the effects of pore structure on reaction mechanism.

In this work, we first investigate monomolecular and bimolecular cracking mechanisms of n-octane over HY and HZSM-5 zeolites by DFT calculation using mGGA-M06L method. Two cracking routes are systematically compared in terms of its apparent energy barrier in the HZSM-5 and HY zeolites. Moreover, the intrinsic reason for the diverse mechanisms in the two zeolites are further investigated on 46T HZSM-5 and 46T HY models. The confinement effect in the pore of zeolite has a profound influence on the stabilities of transition states. The insights in this work will be helpful to understand the effect of confinement on catalytic cracking mechanism of n-alkanes. The pore sizes of most zeolites range from 4 Å to 8 Å<sup>26</sup>. In combination with the conclusion given in this paper and the size of the transition states involved, rough judgments can be made as to whether or not the alkane cracking reaction can be stable in zeolite of different pore-size and the results will be of great importance to the design of highly efficient cracking catalysts.

## **2. Models and methods**

### **2.1. Zeolite models**

The cluster size should apply multicenter spherical cutoffs ( $r \geq 5 \text{ \AA}$ ) based on both centers of the zeolite active site and the adsorbed molecule to within chemical accuracy ( $\pm 1 \text{ kcal/mol}$ )<sup>27</sup>. This cluster not only takes account of the effect of the entire framework

but also reduces the calculation amount at the same time. Therefore, 46T HY and 46T HZSM-5 cluster zeolite models were generated from their lattice structures. The 46T cluster model of H-FAU (in Figure 1) covers the 12-membered window connecting two supercages of faujasite. One aluminum atom substituted for a silicon at T2 site to model a Brønsted acid site. For the ZSM-5 zeolite, the 46T quantum cluster model covers the intersection between the straight channel and the zigzag channel. Silicon at the T12 position was replaced by aluminum to model a Brønsted acid site. During the optimization of the zeolite, only the 8T active region of “(SiO)<sub>3</sub>SiOHA(OSi)<sub>3</sub>” and the adsorbed molecule were allowed to relax while the rest of the structure was fixed at the crystallographic coordinates.

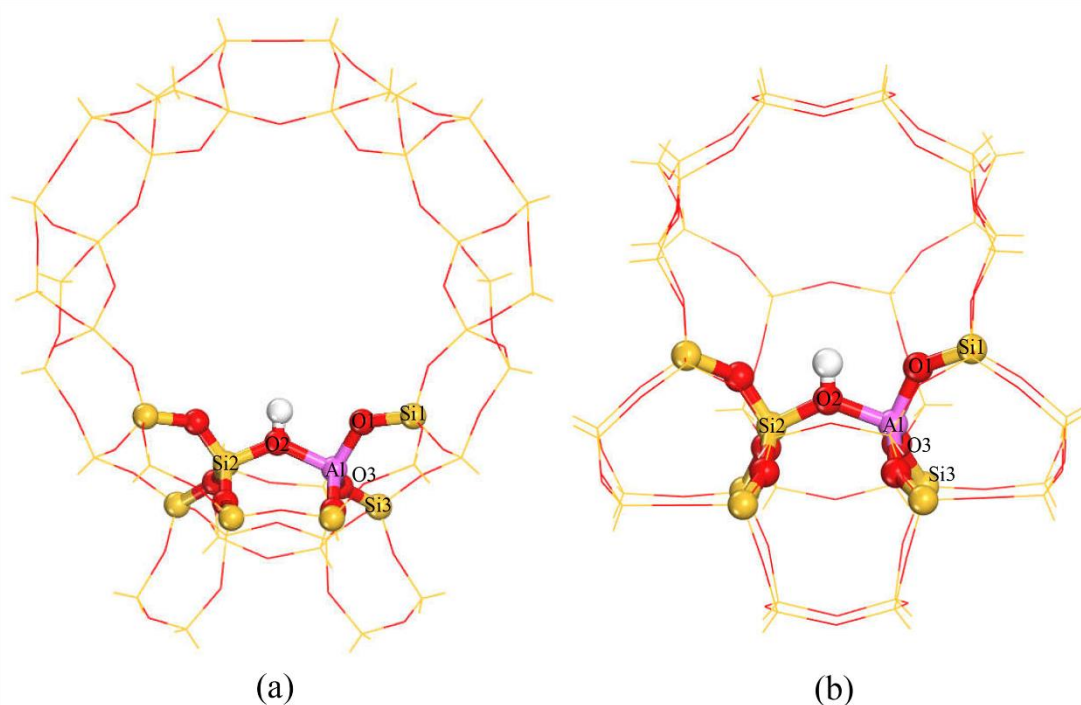


**Figure 1.** Representations of 46T HY (a) and 46T HZSM-5 (b) zeolite cluster models.

## 2.2. Computational details

All calculations were performed with Dmol3 module of Materials Studio 8.0<sup>28, 29</sup>.

The meta-generalized gradient approximation (mGGA) in M06-L parameterization was used in the DFT simulation. The local function (M06-L) is very attractive whose result is comparable to MP2 calculation at a high basis set but at much more affordable computer time<sup>30</sup>. The double numerical plus polarization (DNP) basis set was used with the consideration of the electronic polarization effect. All electron calculation was performed for the complexes, spin unrestricted for the spin state of the system and  $1.0e^{-6}$  for the SCF tolerance. To determine the activation energy for a specific path, the transition state that connected two immediate stable structures through a minimum energy path was identified by complete linear synchronous transit (LST) and quadratic synchronous transit (QST) search methods<sup>31, 32</sup>. The transition-state structures were characterized by only one imaginary frequency corresponding to the normal mode associated with the reaction coordinate. The frequency analysis was performed to check whether the stationary point was the potential minimum. Total energies were corrected by zero-point vibrational energies (ZPE) obtained from frequency calculations. In addition to activation energy, the full Gibbs free activation energies ( $\Delta G_{act}$ ) of each step at 650K, 750K and 850K are also calculated to increase the industrial applicability, because the mild operate temperature of FCC to propylene is the range of 500-560°C<sup>33</sup>. Its calculation process is shown in the Supporting Information. The allowable deviations of the total energy, gradient and displacement were  $1.0 \times 10^{-5}$  Ha, 0.002 Ha/Å and 0.005 Å, respectively.

### 3. Results and discussion

#### 3.1. The monomolecular cracking mechanism of n-octane

Two catalytic cracking routes of n-octane are shown in the Figure 2. The monomolecular cracking mechanism of n-octane is considered to undergo two steps, consisting of n-octane protonation and subsequent decomposition to produce ethylene and n-hexane. In this study, we mainly focus on the C2-C3 bond breaking of n-octane because it can produce ethylene which is one of main representative n-alkane monomolecular cracking products. In the experiment<sup>34</sup>, the selectivity of methane, ethane and ethylene in the product is usually regarded as the selectivity of n-alkane monomolecular cracking reaction. For each intermediate or transition state, optimized geometrical parameters are given in pairs (HZSM-5, HY). Table S1-S6 of optimized geometrical parameters are shown in the Supporting Information. In order to provide a detailed process, Figure S1-S3 for optimized structure of all reaction intermediates and transition states are shown in the Supporting Information.

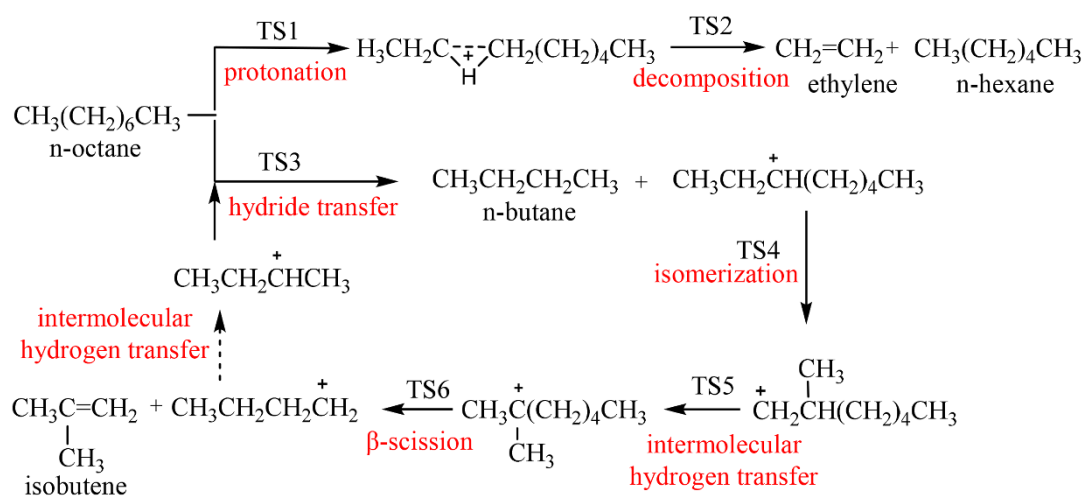


**Figure 2.** Monomolecular and bimolecular cracking pathways of n-octane over zeolites.

### 3.1.1. Protonation of n-octane.

The n-octane molecule is adsorbed on zeolite through the interaction between two methylene carbon atoms and the Brønsted acid site<sup>35</sup>. Alkane activation of monomolecular cracking mechanism usually includes protonation reaction (C-C bond cleavage) and dehydrogenation reaction (C-H bond cleavage)<sup>7</sup>. Most theoretical researchers believe that the protonation reaction is the main initial step for the activation of alkanes because of its lower activation barrier and experimental confirmation. Therefore, dehydrogenation of the alkane is not considered in the paper<sup>10, 24</sup>. Many theoretical studies<sup>36-38</sup> have reported that the non-classical two-electron three-center carbonium ion is the transition state of the protonation reaction. The C-H-C bridged carbonium ion<sup>39</sup> is generated by protonation as the reaction intermediate whose positive charge is delocalized and inaccessible to oxygen atoms of zeolite.

The adsorbed n-octane molecule is protonated at the C2-C3 bond by the acidic proton to form the adsorbed intermediate. Selected geometrical parameters for this step are shown in Table S1 and transition states structures are shown in Figure 3. At the transition state, the C2-H1 and C3-H1 distances are (1.521, 1.289) Å and (1.210, 1.415) Å. The distance of O2-H1 bond is elongated from (0.971, 0.972) Å to (1.810, 1.650) Å and the C2-C3 bond distance is increased to (1.680, 1.698) Å at the same time. The existence of true transition states has been confirmed by frequency calculations resulting in one imaginary frequency at (-773i, -1009i) cm<sup>-1</sup>. This is related to the movement of the acidic proton of zeolite (H1) to the C2-C3 bond of n-octane forming

the adsorbed C2-H1-C3 bridged intermediate. The Mulliken population analysis for the partial atomic charge of the H1 atom are (0.186, 0.162) e showing high hydride characters.

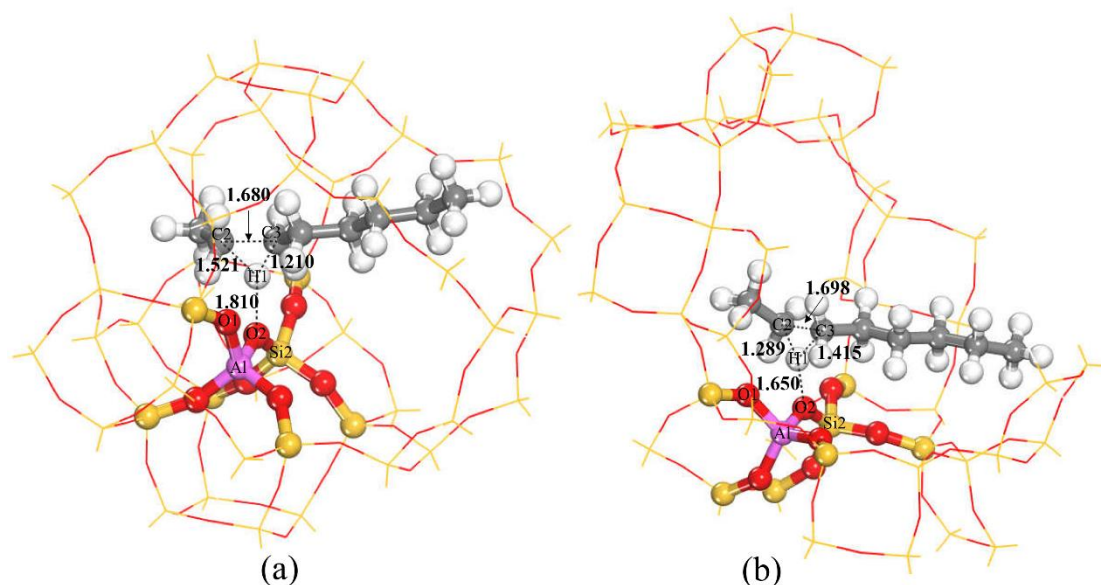


**Figure 3.** Optimized structures of transition states TS1 for protonation reaction of n-octane in the HZSM-5 (a) and HY (b) zeolites.

The adsorption energy of n-octane at 750 K in the HY zeolite is -21.19 kcal/mol, 13.43 kcal/mol smaller than that of HZSM-5 zeolite (-34.62 kcal/mol), which is consistent with calculated results<sup>40</sup>. The Gibbs activation energy of n-octane protonation at 750 K in the HY zeolite is 45.60 kcal/mol, 5.67 kcal/mol higher than that in the HZSM-5 zeolite (39.93 kcal/mol). This means that n-octane has larger stabilizing interaction with HZSM-5 zeolite fragment caused by confinement effect. Because the size of n-octane (3.28×3.36 Å) is fitter with the pore-size of HZSM-5 zeolite (5.3×5.6 and 5.1×5.5 Å) leading to bigger confinement effect compared with HY zeolite (7.4×7.4 Å). In addition to that, the  $\Delta G_{act}$  gap between two zeolites are larger with the increase

of reaction temperature.

### 3.1.2. Decomposition of the octonium intermediate.

The adsorbed 2-C-octonium intermediate is unstable and highly reactive<sup>24</sup>. It can be decomposed back to the adsorbed n-octane with a very small activation barrier. Therefore, it could be extremely difficult to locate this intermediate by experimental means. A more energetic transition state (TS2) is needed to produce ethylene and n-hexane. In this process, the H1 atom moves to C3 atom and the H2 proton next to the C1 atom transfers to oxygen atom of the zeolite framework. As for electronic orbital arrangement, the  $sp^3$ -carbon atom (C2) gradually hybridizes to  $sp^2$  pattern. At the transition state (Figure 4), as shown in Table S2, the C3-H1 bond is reduced to (1.114, 1.109) Å while the C2-C3 and C1-H2 distance is increased to (2.628, 2.932) Å and (1.128, 1.093) Å, respectively. Normal mode analysis reveals one imaginary frequency at (-178i, -242i)  $cm^{-1}$  associated with the TS2, which corresponds to the movement along reaction coordinate. The Gibbs energy barriers of this step at 750 K are 1.19 and 3.46 kcal/mol in the HZSM-5 and HY zeolites, respectively. After the decomposition, an ethylene and n-hexane are produced. The ethylene molecule remains adsorbed on the Bronsted site through a  $\pi$ -bond interaction. Desorption energies of two molecules at 750 K are 30.75 and 20.18 kcal/mol in the HZSM-5 and HY zeolites, respectively.

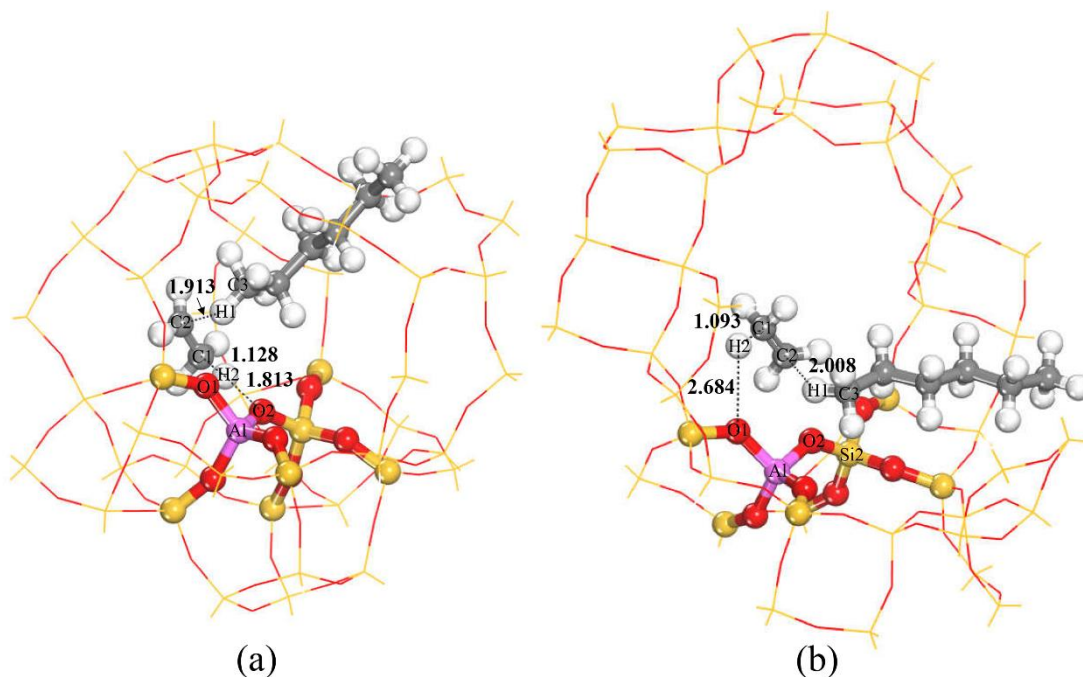


**Figure 4.** Optimized structures of transition states TS2 for decomposition reaction in the HZSM-5 (a) and HY (b) zeolites.

Table 1. The energy barrier ( $\Delta E$ ) and Gibbs free activation barrier ( $\Delta G$ ) for monomolecular cracking mechanism of n-octane in the HZSM-5 and HYzeolite.

parameter	T/K	HZSM-5		HY	
		$\Delta E$	$\Delta G$	$\Delta E$	$\Delta G$
n-octane adsorption	650		-34.45		-21.19
	750	-33.86	-34.62	-20.49	-21.26
	850		-34.80		-21.32
protonation ads1-TS1	650		38.94		43.16
	750	39.96	39.93	36.54	45.60
	850		40.97		48.12
decomposition Int1-TS2	650		2.44		2.16
	750	4.39	1.99	3.79	3.46
	850		1.57		4.49
desorption	650		31.05		19.93
	750	34.30	30.75	22.66	20.18
	850		30.45		20.44

### 3.2. Bimolecular cracking mechanism of n-octane

The classical bimolecular mechanism<sup>41</sup> involves hydride transfer between an alkane and an adsorbed carbenium ion, followed by isomerization and  $\beta$ -scission. In this work, the bimolecular cracking mechanism of n-octane is considered to undergo four steps, consisting of hydride transfer, isomerization, intermolecular hydrogen transfer and  $\beta$ -scission. The bimolecular cracking products of n-octane are isobutene and n-butane which are the main representative products of bimolecular reaction in experiment<sup>8</sup>.

#### 3.2.1. Hydride transfer reaction.

Hydride transfer between an alkane and an alkylcarbenium ion is an important elementary step responsible for bimolecular cracking mechanism of alkane catalyzed by zeolites. To explain this behavior, hydride transfer reaction was found to proceed through a mechanism consisting of two steps<sup>42</sup>. Firstly, the 2-butyl alkoxide bonded to zeolite fragment separates from zeolite fragment and attacks n-octane to form a stable intermediate complex Int3(1) having a bridging hydride. Secondly, the stable intermediate complex decomposed to the product Int3(2) which are 3-octoxide and n-butane. The alkylcarbenium ions are usually formed via protonation of alkenes or  $\beta$ -scission of carbenium ions at the active site of zeolites<sup>43, 44</sup>. The 2-butyl alkoxide here is viewed as one of the product of 2-methyl-heptoxide  $\beta$ -scission step to complete the reaction circle.

Simple carbenium is hardly stable in the channel of zeolite but exist as an

alkylcarbenium ion<sup>45</sup>. By the collision of 2-butyl alkoxide and n-octane, a loose complex is formed. The C1-O1 bond of 2-butyl alkoxide is shortened by (0.052, 0.002) Å, indicating the bulky size of loose complex compared to the pore of HZSM-5. To form the H-shared intermediate, the 2-butyl alkoxide separates from zeolite fragment and turns into a high-activity carbenium. Then it attacks the n-octane to share its hydrogen atom. As shown in Table S3, the distance of C1-O1 bond is increased to (2.781, 2.789) Å from (1.537, 1.588) Å, and C1-H distance is shortened to (1.257, 1.423) Å from (2.336, 2.965) Å at the same time. At the transition state TS3 (Figure 5), the 2-butyl alkoxide has already generated the 2-butyl carbenium ion, but the H-shared complex has not formed yet, in which the distance of C1-O1 bond and C1-H bond are (2.705, 2.669) Å and (1.319, 1.583) Å, respectively. The only imaginary is found at (-69i, -72i) cm<sup>-1</sup>, related to the movement of the C1 atom of 2-butyl carbenium to the H proton of n-octane. The H-shared intermediate (Int3(1)) is highly unstable and easily decomposes to the product without any reaction barrier<sup>46</sup>, so we just calculated the second step of hydride transfer in HZSM-5 zeolite whose result shows that there is no energy barrier. The detail information of second step is shown in the Figure S2 and Table S7 in the Supporting Information. The Int3(2) is the product of the second step of hydride transfer reaction which are 3-octoxide and n-butane.

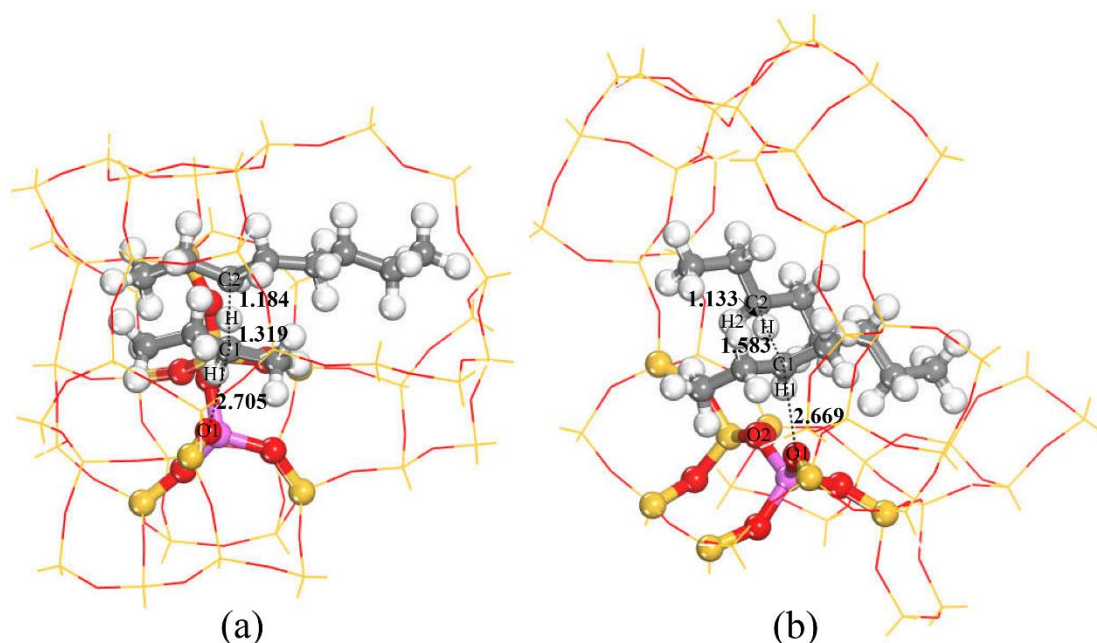


**Figure 5.** Optimized structures of transition states TS3 for hydride transfer reaction in the HZSM-5 (a) and HY (b) zeolites.

In the HY zeolite, the entry energy associated with the n-octane moving from the gas phase into the zeolite pore is highly exothermic (-21.72 kcal/mol), while the n-octane need extra energy (13.31 kcal/mol) into the pore of HZSM-5 from the gas phase. Because there is the competition between dispersion stabilization and electrostatic repulsion in the pore of zeolite. HY zeolite fragment generates bigger dispersion stabilization than electrostatic repulsion for loose complex, while the effect of electrostatic repulsion in HZSM-5 zeolite fragment destabilize this loose complex significantly. Besides, the Gibbs energy barrier of this step at 750K in the HY zeolite is 8.13 kcal/mol, lower than that in the HZSM-5 zeolite (9.81 kcal/mol). The estimated size of TS3 is approximately 4.30×5.28 Å. Compared with the pore-size of HZSM-5 (5.3×5.6 and 5.1×5.5 Å), TS3 is much fitter with HY zeolite (7.4×7.4 Å) leading to stronger dispersion stabilization from the zeolite fragment. Therefore, transition states

can be effectively stabilized if its size is comparable to the pore-size of zeolites, which is consistent with theoretical result<sup>47</sup>.

### 3.2.2. Isomerization reaction of 3-octoxide.

Three possible mechanisms have been proposed for the skeletal isomerization of hydrocarbon, monomolecular<sup>48, 49</sup>, bimolecular<sup>50</sup> and pseudo-monomolecular<sup>51</sup> mechanisms. Among these three mechanisms, the monomolecular mechanism is currently considered to be the predominant mechanism for the isomerization, whereas the bimolecular mechanism is mainly responsible for the formation of byproducts<sup>52, 53</sup>.

In this isomerization process, the 3-octoxide produce 2-methyl-1-heptoxide in which the methyl group (C1) is transferred from C2 to C3 via the transition of protonated cyclopropyl cation. At the transition state (Table S4 and Figure 6), the distance of C1–C2 bond and C1–C3 bond are (1.897, 1.861) Å and (1.687, 1.710) Å, respectively. The Mulliken population analysis indicates a partial charge of (+0.867, +0.901) e on the cyclopropyl cation transition state in which the C3 position carries the most positive charge. The calculated imaginary frequency is (-369i, -385i) cm<sup>-1</sup>, corresponding to the movement of the methyl group (C1) from C2 to C3 atom. After the transition, C1 is bound to C3 with a bond length of (1.540, 1.533) Å and the C1–C2 bond is broken. Simultaneously, 2-methyl-1-heptoxide is formed whose C2 becomes bound to the lattice O1 with a bond length of (1.587, 1.559) Å.

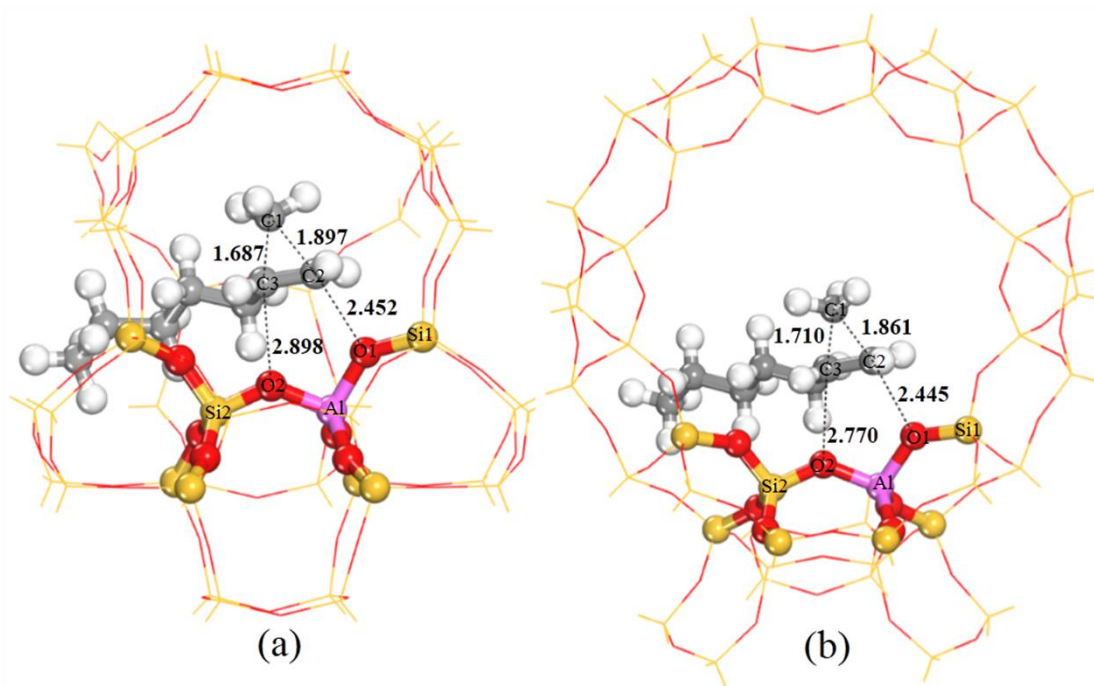


**Figure 6.** Optimized structures of transition states TS4 for isomerization reaction in the HZSM-5 (a) and HY (b) zeolites.

The Gibbs energy barriers of this step at 750K in the HY zeolite is 15.43 kcal/mol, 10.72 kcal/mol higher than that in the HZSM-5 zeolite (4.71 kcal/mol), meaning that isomerization reaction is easier to proceed in the HZSM-5. The estimated size of transition state TS4 is  $3.61 \times 3.82$  Å. Compared with the HZSM-5 ( $5.3 \times 5.6$  and  $5.1 \times 5.5$  Å), the large supercage ( $7.4 \times 7.4$  Å) of the HY zeolite has limited stabilizing effect on the TS4 resulting in larger energy barrier for this step.

### 3.2.3. Intermolecular hydrogen transfer reaction.

The 2-methyl-1-heptoxide and 2-methyl-2-heptyl cation could convert into each other by intermolecular hydrogen transfer reaction. In this process, the C-O bond is shifted to adjacent carbon and a proton is transferred in the opposite direction simultaneously. The optimized transition-state structure is illustrated in Figure 7 and

Table S5. Both C1 and C2 atoms are already  $sp^2$  hybridized. The distance of C2–H and C1–H bonds are (1.174, 1.154) Å and (1.698, 1.889) Å. The transition-state model has Mulliken charge of (+0.811, +0.754) e. The terminal C1 position has the most positive charge, indicating that the hydride shift from the C2 to C1 atom is still in an early stage. From the vibrational analysis of the transition state TS5, there is one imaginary frequency (-380i, -205i)  $cm^{-1}$  corresponding to the movement of the H atom from the C2 to C1 carbon atom. This suggests that the proton should not be directly deprotonated back to the zeolite but be shifted to the positively charged primary carbon (C1). After the transition state, the 2-methyl-2-heptyl cation is produced as an almost planar structure in which the C–C bond lengths are approximately equivalent. The closest distance from the tertiary C2 atom to the zeolite O2 atom are (3.152, 2.842) Å. The 2-methyl-2-heptyl cation is stabilized in the zeolite pore by the electrostatic interactions as well as the hydrogen bonds among the cation methyl group and the zeolite oxygen atoms.

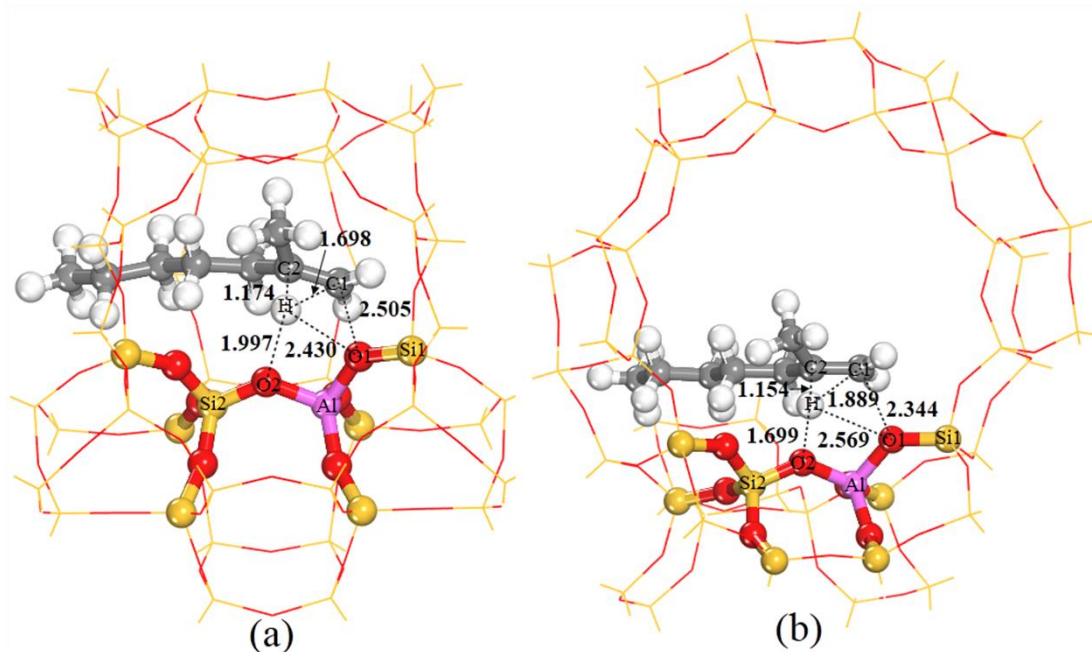


**Figure 7.** Optimized structures of transition states TS5 for intermolecular hydrogen transfer reaction in the HZSM-5 (a) and HY (b) zeolites.

The estimated size of transition-state TS5 is  $3.68 \times 3.99$  Å, similar to that of TS4. The Gibbs energy barriers of this step at 750 K are 0.08 and 4.73 kcal/mol in the HZSM-5 and HY zeolites, respectively. Due to its appropriate size, HZSM-5 zeolite has larger confinement effect on the TS5 and decreases its energy barrier more effectively than HY zeolite. In addition, the step can release energy of (21.38, 15.64) kcal/mol, so the 2-methyl-2-heptyl cation exist more stably in the pore of zeolites compared to 2-methyl-1-heptoxide.

### 3.2.4. $\beta$ -scission reaction

Carbeniums exist as true reaction intermediates in zeolite-catalyzed processes only when their positive charges are hardly accessible to framework oxygen atoms<sup>43, 54</sup>. In this case, the carbenium usually adsorbs physically on the zeolite fragment and the  $C^+$

atom is already  $sp^2$  hybridized.  $\beta$ -scission begins with the elongation of the bond in the  $\beta$ -position from  $C^+$ . The transition-state structure is achieved once the  $\alpha$ -C and  $\beta$ -C atoms become fully  $sp^2$  hybridized. And then two fragments, an olefin and another carbenium, are formed. This carbenium usually form an alkoxide with the alkyl group covalently bonded to the framework oxygen, because alkoxy species have been found to be important long-lived intermediates in the reaction on zeolites<sup>55</sup>.

In this  $\beta$ -scission process, the cleavage of C2-C3 bond is observed and the 2-methyl-heptoxide is separated into two moieties, 2-methyl propene and butoxide. Figure 8 shows the optimized structures of the transition states TS6. The cleavage of C2-C3 bond has already occurred and C2 and C3 atoms become fully  $sp^2$  hybridized. However, as shown in Table S6, new O3-C3 bonds are not completely formed yet, as shown by its (3.236, 2.075) Å. The new alkene molecule is formed approximately because the new C1=C2 bond length (1.348 Å, 1.345 Å) is very close to the normal C=C bond length (1.331 Å) of 2-methyl propene. Only one imaginary frequency has been calculated at (-255.32i, -195.89i)  $cm^{-1}$ , corresponding to the movement of the C3 atom from the C2 atom of 2-methyl-2-heptyl cation to O3 atom of zeolite fragment. After the transition state, the optimized O3-C3 distance is reduced to ca. (1.529, 1.552) Å.

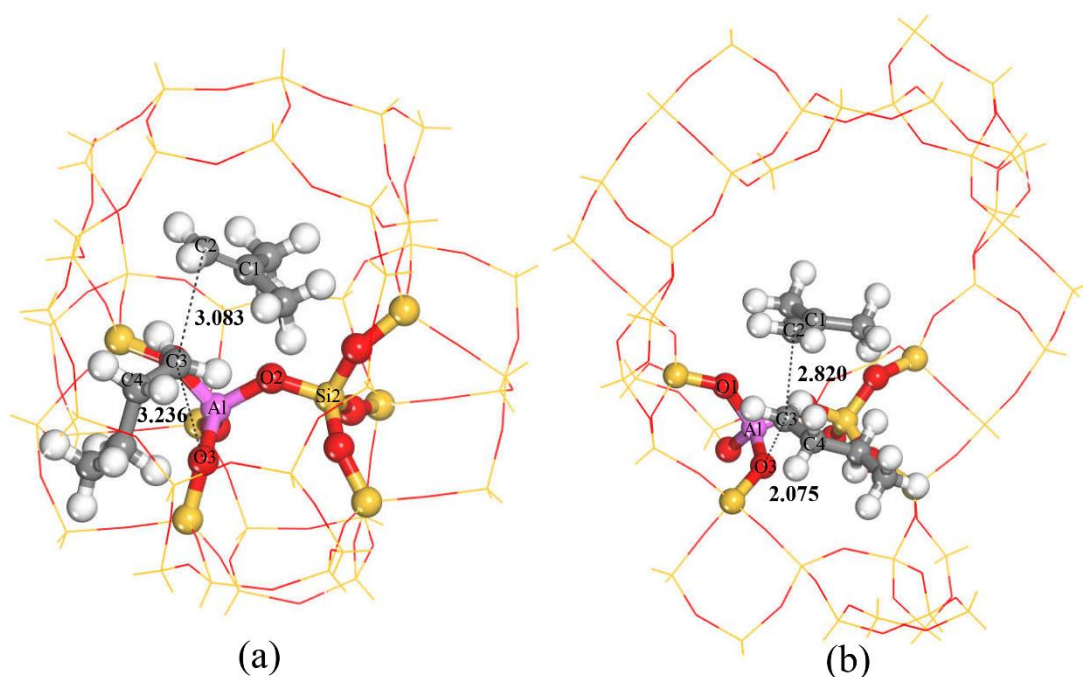


**Figure 8.** Optimized structures of transition states TS6 for the  $\beta$ -scission reaction in the HZSM-5 (a) and HY (b) zeolites.

The Gibbs energy barriers of  $\beta$ -scission at 750 K are 46.75 and 22.89 kcal/mol in the HZSM-5 and HY zeolites, respectively, which are consistent with recent theoretical study<sup>56</sup>. Compared with HY zeolite, the stabilizing effect on the TS6 from the HZSM-5 zeolite fragment ( $5.3 \times 5.6$  and  $5.1 \times 5.5$  Å) becomes less predominant due to its bulky size ( $4.77 \times 5.46$  Å) and the destabilizing effect from steric constraint is increasing remarkably leading to a higher energy barrier. In addition to that, the gap of  $\Delta G_{\text{act}}$  in both zeolites at 750 K is 23.86 kcal/mol, 1.1 kcal/mol larger than that at 650 K. This means that the gap of  $\beta$ -scission in both zeolites increases with raising reaction temperature. The alkene products are desorbed with the energy needed of 20.29 and 10.62 kcal/mol from the pores of HZSM-5 and HY zeolites, respectively.

Table 2. The energy barrier ( $\Delta E$ ) and Gibbs free activation barrier ( $\Delta G$ ) for bimolecular cracking mechanism of n-octane in the HZSM-5 and HY zeolite.

parameter	T/K	HZSM-5		HY	
		$\Delta E$	$\Delta G$	$\Delta E$	$\Delta G$
n-octane adsorption	650		12.38		-21.88
	750	10.17	13.31	-20.53	-21.72
	850		14.32		-21.54
hydride transfer Ads2-TS3	650		10.45		7.57
	750	16.67	9.81	11.16	8.13
	850		9.15		8.72
n-butane desorption	650		-4.68		17.73
	750	-3.74	-4.93	18.67	17.48
	850		-5.17		17.24
isomerization Int4-TS4	650		4.96		15.20
	750	8.61	4.71	17.16	15.43
	850		4.47		15.69
intermolecular hydrogen transfer Int5-TS5	650		0.99		5.14
	750	2.07	0.08	6.95	4.73
	850		-0.80		4.31
$\beta$ -scission Int7-TS6	650		45.15		22.38
	750	42.20	46.75	25.86	22.89
	850		48.47		23.47
Isobutylene desorption	650		20.14		10.63
	750	19.30	20.29	10.67	10.62
	850		20.43		10.61

### 3.3. Comparison of monomolecular and bimolecular mechanisms.

As described above, we mainly studied monomolecular and bimolecular cracking mechanisms of the n-octane over zeolites in FCC process. The free energy profiles of monomolecular and bimolecular mechanisms in zeolites are sketched in Figure 9 and Figure 10, respectively. From Figure 9, it can be seen that the overall apparent reaction barrier for the monomolecular cracking reaction is considered to be the energy difference between the adsorbed n-octane and the transition state (TS1) of protonation

step. It is calculated to be 5.30 and 24.34 kcal/mol in the HZSM-5 and HY zeolites, respectively. Besides, the transition states and intermediates in HZSM-5 are 10-20 kcal/mol lower in energies than those stationary points in HY zeolites due to different confinement effect. Furthermore, in the HZSM-5 zeolite, the apparent reaction barrier for the monomolecular cracking reaction (5.30 kcal/mol) is much lower than that for bimolecular cracking reaction (23.12 kcal/mol). Therefore, the monomolecular cracking mechanism of n-octane is predominant in the HZSM-5 zeolite, which is confirmed by the experimental results<sup>57</sup>.

In the bimolecular cracking reaction, it is observed that the apparent reaction barrier at 750 K in the ZSM-5 zeolite is the energy difference between the adsorbed n-octane and the TS3 of hydride transfer step which is 23.12 kcal/mol. The value is 16.17 kcal/mol higher than that (6.95 kcal/mol) in the HY zeolite whose energy difference is between the adsorbed n-octane and the TS4 of isomerization step. What's more, in the HY zeolite, the apparent reaction barrier for the bimolecular cracking reaction (6.95 kcal/mol) is much lower than that for monomolecular cracking reaction (24.34 kcal/mol). This means bimolecular cracking mechanism is predominant in the cracking of n-octane in HY zeolite. This theoretical result is consistent with the experimental yield of n-alkanes.<sup>9</sup>

The above results can be explained by the confinement effect on the transition state from zeolite fragment. Greater stabilizing confinement effect on the transition state decrease its energy barrier more effectively. The transition state TS1 in the pore of HY

zeolite occupies a small space and has seldom electrostatic interaction with the upper zeolite framework, meaning the limited confinement effect. However, the transition state TS4 in the pore of HY zeolite occupy appropriate pore space and electrostatic interaction between transition state and zeolite fragment is effective, so confinement effect can greatly stabilize these transition states leading to smaller energy barrier. As in the aforementioned discussion, strong steric repulsion is present for n-octane adsorbed on the 2-butyl oxide complex in the ZSM-5 zeolite which will result in the difficult follow-up reaction. Therefore, the confinement effect plays an important role for decreasing energy barrier, especially considering the aimed product selectivity. When the size of transition state is fitted perfectly into the pore of zeolite, the confinement effect can stabilize the transition state effectively thereby decrease its energy barrier and then has an impact on the reaction route selectivity.

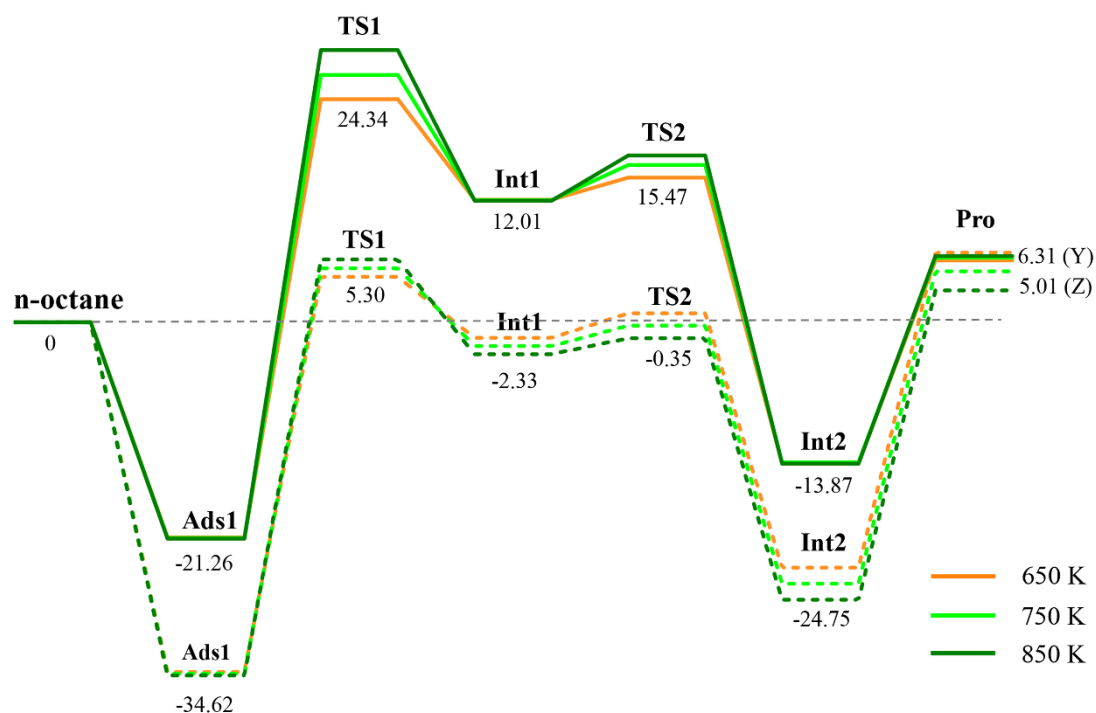


**Figure 9.** The Gibbs free energy for monomolecular cracking mechanism at 650K, 750K and

850K in the HZSM-5 (dash line) and HY (solid line) zeolites. (The energy number labeled at 750K)

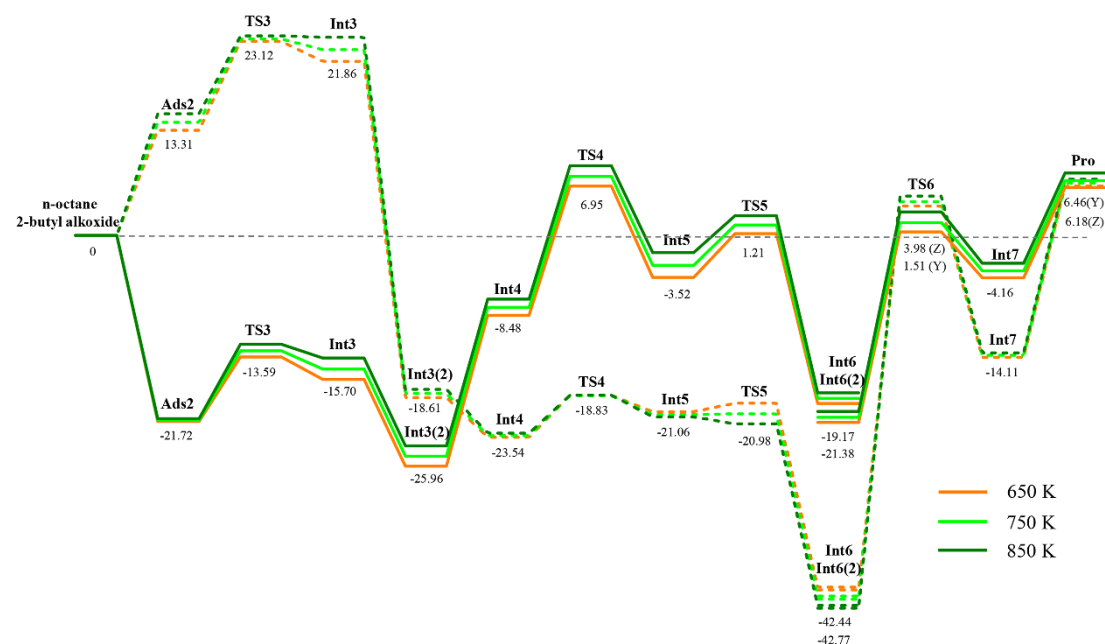


**Figure 10.** The Gibbs free energy for bimolecular cracking mechanism at 650K, 750K and 850K in the HZSM-5 (dash line) and HY (solid line) zeolites. (The energy number labeled at 750K)

## 4. Conclusion

DFT calculation using mGGA-M06-L function was carried out to characterize cracking reaction mechanisms of n-octane in the 46T HY and 46T HZSM-5 cluster models. The overall apparent reaction barrier for the monomolecular cracking reaction at 750 K in the HZSM-5 zeolite is 5.30 kcal/mol, much lower than that (23.12 kcal/mol) for bimolecular cracking reaction, while the apparent reaction barriers for the monomolecular cracking reaction (24.34 kcal/mol) in the HY zeolite are 17.39 kcal/mol higher than that (6.95 kcal/mol) for bimolecular cracking reaction. Therefore,

bimolecular mechanism is predominant in the cracking of n-octane in the HY zeolite while monomolecular mechanism is predominant in the HZSM-5 zeolite.

The dominant mechanism in the pores of the HZSM-5 and HY zeolites is distinct mainly because of the different confinement effect. The confinement effect can decrease the energy barrier effectively if the size of confined molecules involved in reactions (i.e., reactants and transition states) is comparable to the pore-size of zeolite. The diameter sizes of n-alkane and methyl-alkane are in the range of 3.2 to 4.0 Å, which is compatible with the pore-size of HZSM-5. The transition state can be well stabilized by the pore of HZSM-5 and then energy barrier of the reaction can be effectively decreased. In addition, the limited pore of HZSM-5 has the difficulty in accommodating two molecule fragments at the same time in which there is usually strong steric repulsion, while two molecule fragments as transition state can be well stabilized by the pore of HY zeolite. The confinement effect plays an important role in the stabilities of reactants and transition states, and then influences n-octane catalytic cracking process. The results may provide a theoretical guide for the design and modification of solid acid catalysts in the petrochemical industry.

## **Acknowledgments**

This work was supported by the National Science Foundation of China (Grant Nos. U1462205, 21476263, 21606254), Key research and development plan of Shandong Province (2017GSF17126), Natural Science Foundation of Shandong Province

(ZR2016BB16), Independent innovation foundation of Qingdao (17-1-1-18-jch), Fundamental Research Funds for the Central Universities (18CX02130A, 18CX02014A) and Graduate Innovation Project (YCX2017037).

## **Supporting Information Available**

Data of all structural parameters for optimized transition states and intermediates in the HZSM-5 and HY zeolites. Figures for two cracking reaction step including TS and intermediates. The calculating procedure of Gibbs free energy for all transition state and intermediates.

## References

- (1) Ha, Y.; Guo, B.; Li, Y. Sensitivity and economic analysis of a catalytic distillation process for alkylation desulfurization of fluid catalytic cracking (FCC) gasoline. *J. Chem. Technol. Biot.* **2016**, *91*, 490-506.
- (2) Gueudré, L.; Chapon, F.; Mirodatos, C.; Schuurman, Y.; Venderbosch, R.; Jordan, E.; Wellach, S.; Gutierrez, R. M. Optimizing the bio-gasoline quantity and quality in fluid catalytic cracking co-refining. *Fuel* **2017**, *192*, 60-70.
- (3) Yaluris, G.; Rekoske, J.; Aparicio, L.; Madon, R.; Dumesic, J. Isobutane cracking over Y-zeolites: I. Development of a kinetic-model. *J. Catal.* **1995**, *153*, 54-64.
- (4) Kotrel, S.; Knözinger, H.; Gates, B. The Haag–Dessau mechanism of protolytic cracking of alkanes. *Micropor. Mesopor. Mat.* **2000**, *35*, 11-20.
- (5) Kubo, K.; Iida, H.; Namba, S.; Igarashi, A. Selective formation of light olefin by n-heptane cracking over HZSM-5 at high temperatures. *Micropor. Mesopor. Mat.* **2012**, *149*, 126-133.
- (6) Corma, A.; Mengual, J.; Miguel, P. J. Catalytic cracking of n-alkane naphtha: the impact of olefin addition and active sites differentiation. *J. Catal.* **2015**, *330*, 520-532.
- (7) Hou, X.; Qiu, Y.; Zhang, X.; Liu, G. Analysis of reaction pathways for n-pentane cracking over zeolites to produce light olefins. *Chem. Eng. J.* **2017**, *307*, 372-381.
- (8) Wielers, A.; Vaarkamp, M.; Post, M. Relation between properties and performance of zeolites in paraffin cracking. *J. Catal.* **1991**, *127*, 51-66.
- (9) Corma, A.; Miguel, P. J.; Orchilles, A. V. The role of reaction temperature and

- cracking catalyst characteristics in determining the relative rates of protolytic cracking, chain propagation, and hydrogen transfer. *J. Catal.* **1994**, *145*, 171-180.
- (10) Chu, Y.; Han, B.; Fang, H.; Zheng, A.; Deng, F. Influence of acid strength on the reactivity of alkane activation on solid acid catalysts: A theoretical calculation study. *Micropor. Mesopor. Mat.* **2012**, *151*, 241-249.
- (11) Liu, C.; Li, G.; Hensen, E. J.; Pidko, E. A. Relationship between acidity and catalytic reactivity of faujasite zeolite: A periodic DFT study. *J. Catal.* **2016**, *344*, 570-577.
- (12) Silaghi, M. C.; Chizallet, C.; Sauer, J.; Raybaud, P. Dealumination mechanisms of zeolites and extra-framework aluminum confinement. *J. Catal.* **2016**, *339*, 242-255.
- (13) Wang, C.-M.; Brogaard, R. Y.; Xie, Z.-K.; Studt, F. Transition-state scaling relations in zeolite catalysis: influence of framework topology and acid-site reactivity. *Catal. Sci. Technol.* **2015**, *5*, 2814-2820.
- (14) Jones, A. J.; Zones, S. I.; Iglesia, E. Implications of transition state confinement within small voids for acid catalysis. *J. Phys. Chem. C* **2014**, *118*, 17787-17800.
- (15) Mazar, M.; Al-Hashimi, S.; Bhan, A.; Cococcioni, M. Methylation of ethene by surface methoxides: A periodic PBE+ D study across zeolites. *J. Phys. Chem. C* **2012**, *116*, 19385-19395.
- (16) Simonetti, D. A.; Carr, R. T.; Iglesia, E. Acid strength and solvation effects on methylation, hydride transfer, and isomerization rates during catalytic homologation of C 1 species. *J. Catal.* **2012**, *285*, 19-30.

- (17) Xu, B.; Sievers, C.; Hong, S. B.; Prins, R.; van Bokhoven, J. A. Catalytic activity of Brønsted acid sites in zeolites: Intrinsic activity, rate-limiting step, and influence of the local structure of the acid sites. *J. Catal.* **2006**, *244*, 163-168.
- (18) Lesthaeghe, D.; Sterck, B. D.; Speybroeck, V. V.; Marin, G. B.; Waroquier, M. Zeolite Shape-Selectivity in the gem-Methylation of Aromatic Hydrocarbons. *Angew. Chem. Int. Ed.* **2007**, *46*, 1311-1314.
- (19) Clark, L. A.; Sierka, M.; Sauer, J. Computational elucidation of the transition state shape selectivity phenomenon. *J. Amer. Chem. Soc.* **2004**, *126*, 936-947.
- (20) Inagaki, S.; Shinoda, S.; Hayashi, S.; Wakihara, T.; Yamazaki, H.; Kondo, J. N.; Kubota, Y. Improvement in the catalytic properties of ZSM-5 zeolite nanoparticles via mechanochemical and chemical modifications. *Catal. Sci. Technol.* **2016**, *6*, 2598-2604.
- (21) Gong, T.; Qin, L.; Lu, J.; Feng, H. ZnO modified ZSM-5 and Y zeolites fabricated by atomic layer deposition for propane conversion. *Phys. Chem. Chem. Phys.* **2016**, *18*, 601-614.
- (22) Fang, H.; Zheng, A.; Xu, J.; Li, S.; Chu, Y.; Chen, L.; Deng, F. Theoretical investigation of the effects of the zeolite framework on the stability of carbenium ions. *J. Phys. Chem. C* **2011**, *115*, 7429-7439.
- (23) Milas, I.; Nascimento, M. A. C. A density functional study on the effect of the zeolite cavity on its catalytic activity: The dehydrogenation and cracking reactions of isobutane over HZSM-5 and HY zeolites. *Chem. Phys. Lett.* **2006**, *418*, 368-372.

- (24) Maihom, T.; Pantu, P.; Tachakritikul, C.; Probst, M. Limtrakul, J. Effect of the zeolite nanocavity on the reaction mechanism of n-hexane cracking: A density functional theory study. *J. Phys. Chem. C* **2010**, *114*, 7850-7856.
- (25) Yeh, Y.-H.; Gorte, R.; Rangarajan, J. S.; Mavrikakis, M. Adsorption of Small Alkanes on ZSM-5 Zeolites: Influence of Brønsted Sites. *J. Phys. Chem. C* **2016**, *120*, 12132-12138.
- (26) Smit, B.; Maesen, T. L. M. Towards a molecular understanding of shape selectivity. *Nature* **2008**, *451* (7179), 671.
- (27) Migues, A. N.; Muskat, A.; Auerbach, S. M.; Sherman, W.; Vaitheeswaran, S. On the Rational Design of Zeolite Clusters. *ACS Catal.* **2015**, *5*, 2859-2865.
- (28) Delley, B. From molecules to solids with the DMol3 approach. *J. Chem. Phys.* **2000**, *113*, 7756-7764.
- (29) Delley, B. An all - electron numerical method for solving the local density functional for polyatomic molecules. *J. Chem. Phys.* **1990**, *92*, 508-517.
- (30) Zhao, Y.; Truhlar, D. G. Density functionals with broad applicability in chemistry. *Acc. Chem. Res.* **2008**, *41*, 157-167.
- (31) Bell, S.; Crighton, J. S. Locating transition states. *J. Chem. Phys.* **1984**, *80*, 2464-2475.
- (32) Fischer, S.; Karplus, M. Conjugate peak refinement: an algorithm for finding reaction paths and accurate transition states in systems with many degrees of freedom. *Chem. Phys. Lett.* **1992**, *194*, 252-261.
- (33) Li, X.; Li, C.; Zhang, J.; Yang, C.; Shan, H. Effects of temperature and catalyst to

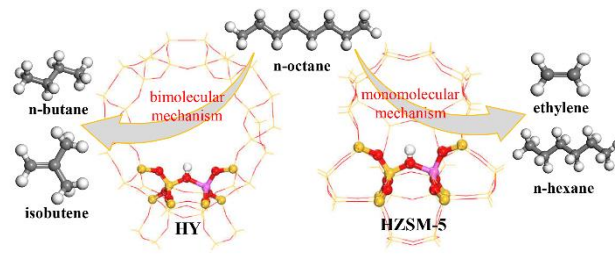
- oil weight ratio on the catalytic conversion of heavy oil to propylene using ZSM-5 and USY catalysts. *J. Nat. Gas Chem.* **2007**, 16(1), 92-99.
- (34) Kubo, K.; Iida, H.; Namba, S.; Igarashi, A. Selective formation of light olefin by n-heptane cracking over HZSM-5 at high temperatures. *Micropor. Mesopor. Mat.* **2012**, 149, 126-133.
- (35) Stöcker, M. Gas phase catalysis by zeolites. *Micropor. Mesopor. Mat.* **2005**, 82, 257-292.
- (36) Blaszkowski, S.; Nascimento, M.; Santen, R. V. Activation of CH and CC bonds by an acidic zeolite: a density functional study. *J. Phys. Chem.* **1996**, 100, 3463-3472.
- (37) Zheng, X.; Blowers, P. Reactivity of alkanes on zeolites: A computational study of propane conversion reactions. *J. Phys. Chem. A* **2005**, 109, 10734-10741.
- (38) Tranca, D. C.; Zimmerman, P. M.; Gomes, J.; Lambrecht, D.; Keil, F. J.; Head-Gordon, M.; Bell, A. T. Hexane Cracking on ZSM-5 and Faujasite Zeolites: a QM/MM/QCT Study. *J. Phys. Chem. C* **2015**, 119, 28836-28853.
- (39) Boronat, M.; Viruela, P.; Corma, A. Ab initio and density-functional theory study of zeolite-catalyzed hydrocarbon reactions: hydride transfer, alkylation and disproportionation. *Phys. Chem. Chem. Phys.* **2000**, 2, 3327-3333.
- (40) Moor, B. A. D.; Reyniers, M.-F.; Gobin, O. C.; Lercher, J. A.; Marin, G. B. Adsorption of C<sub>2</sub>–C<sub>8</sub> n-Alkanes in Zeolites. *J. Phys. Chem. C* **2010**, 115, 1204-1219.
- (41) Boronat, M.; Viruela, P.; Corma, A. Theoretical study of bimolecular reactions

- between carbenium ions and paraffins: The proposal of a common intermediate for hydride transfer, disproportionation, dehydrogenation, and alkylation. *J. Phys. Chem. B* **1999**, *103*, 7809-7821.
- (42) Boronat, M.; Viruela, P.; Corma, A. Theoretical study on the mechanism of the hydride transfer reaction between alkanes and alkylcarbenium ions. *J. Phys. Chem. B* **1997**, *101*, 10069-10074.
- (43) Kazansky, V.; Senchenya, I. Quantum chemical study of the electronic structure and geometry of surface alkoxy groups as probable active intermediates of heterogeneous acidic catalysts: What are the adsorbed carbenium ions? *J. Catal.* **1989**, *119*, 108-120.
- (44) Hwang, A.; Prieto-Centurion D.; Bhan, A. Isotopic tracer studies of methanol-to-olefins conversion over HSAPO-34: The role of the olefins-based catalytic cycle. *J. Catal.* **2016**, *337*, 52-56.
- (45) Boronat, M.; Corma, A. Are carbenium and carbonium ions reaction intermediates in zeolite-catalyzed reactions? *Appl. Catal. A-Gen.* **2008**, *336*, 2-10.
- (46) Boronat, M.; Viruela, P.; Corma, A. A theoretical study of the mechanism of the hydride transfer reaction between alkanes and alkenes catalyzed by an acidic zeolite. *J. Phys. Chem. A* **1998**, *102* (48), 9863-9868.
- (47) Chu, Y.; Han, B.; Zheng, A.; Deng, F. Influence of acid strength and confinement effect on the ethylene dimerization reaction over solid acid catalysts: A theoretical calculation study. *J. Phys. Chem. C* **2012**, *116*, 12687-12695.
- (48) Wattanakit, C.; Nokbin, S.; Boekfa, B.; Pantu, P.; Limtrakul, J. Skeletal

- isomerization of 1-butene over ferrierite zeolite: A quantum chemical analysis of structures and reaction mechanisms. *J. Phys. Chem. C* **2012**, *116*, 5654-5663.
- (49) Kangas, M.; Kumar, N.; Harlin, E.; Salmi, T.; Murzin, D. Y. Skeletal Isomerization of Butene in Fixed Beds. 1. Experimental Investigation and Structure–Performance Effects. *Ind. Eng. Chem. Res.* **2008**, *47*, 5402-5412.
- (50) Menorval, B. D.; Ayrault, P.; Gnep, N.; Guisnet, M. n-Butene skeletal isomerization over HFER zeolites: Influence of Si/Al ratio and of carbonaceous deposits. *Appl. Catal. A-Gen.* **2006**, *304*, 1-13.
- (51) Petkovic, L. a. M.; Larsen, G. Linear butenes from isobutene over H-ferrierite: In situ studies using an oscillating balance reactor. *J. Catal.* **2000**, *191*, 1-11.
- (52) Domokos, L.; Lefferts, L.; Seshan, K.; Lercher, J. Isomerization of Linear Butenes to iso-Butene over Medium Pore Zeolites: I. Kinetic Aspects of the Reaction over H-FER. *J. Catal.* **2001**, *197*, 68-80.
- (53) He, M.; Zhang, J.; Liu, R.; Sun, X. L.; Chen, B.H.; Wang, Y. G. Density functional theory studies on the skeletal isomerization of 1-butene catalyzed by HZSM-23 and HZSM-48 zeolites. *RSC Adv.* **2017**, *7*, 9251-9257.
- (54) Mazar, M. N.; Al-Hashimi, S.; Cococcioni, M.; Bhan, A.  $\beta$ -Scission of olefins on acidic zeolites: a periodic PBE-D study in H-ZSM-5. *J. Phys. Chem. C* **2013**, *117*, 23609-23620.
- (55) Guo, Y. H.; Pu, M.; Chen, B. H.; Cao, F. Theoretical study on the cracking reaction catalyzed by a solid acid with zeolitic structure: The catalytic cracking of 1-hexene on the surface of H-ZSM-5. *Appl. Catal. A-Gen.* **2013**, *455*, 65-70.

- (56) Sun, Y. X.; Yang, J.; Zhao, L.F.; Dai, J. X.; Sun, H. A two-layer ONIOM study on initial reactions of catalytic cracking of 1-butene to produce propene and ethene over HZSM-5 and HFAU zeolites. *J. Phys. Chem. C* **2010**, *114*, 5975-5984.
- (57) Krannila, H.; Haag, W.; Gates, B. Monomolecular and bimolecular mechanisms of paraffin cracking: n-butane cracking catalyzed by HZSM-5. *J. Catal.* **1992**, *135* (1), 115-124.

# TOC Graphic



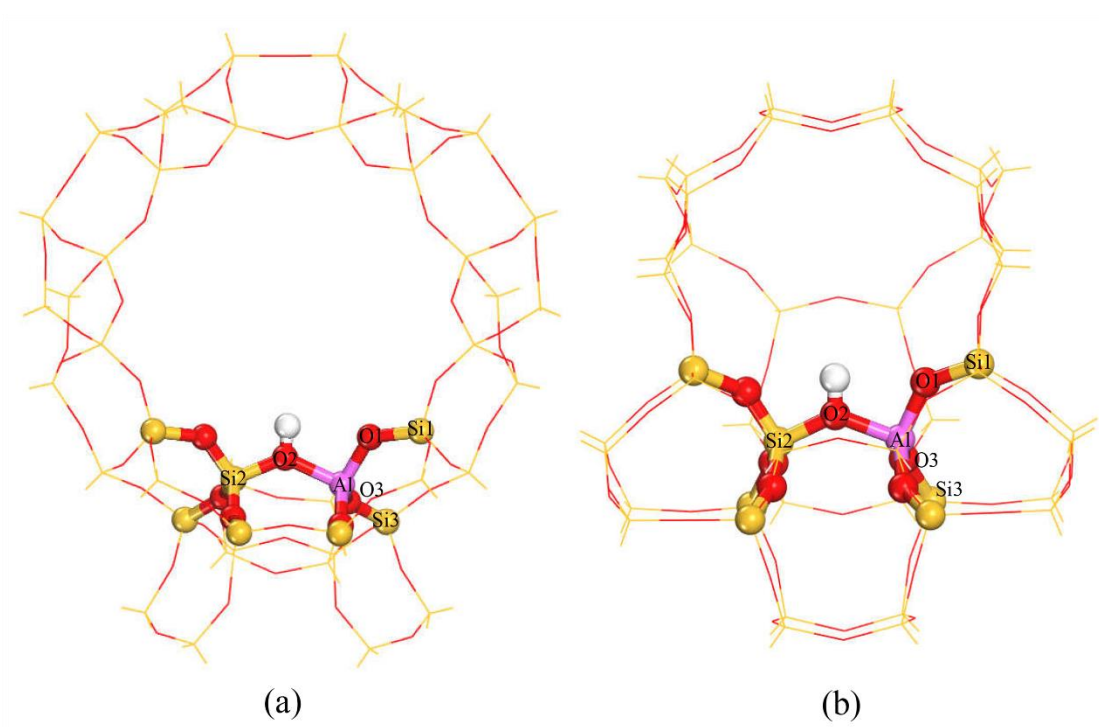


**Figure 1.** Representations of 46T HY (a) and 46T HZSM-5 (b) zeolite cluster models.

175×113 mm (500×500 DPI)

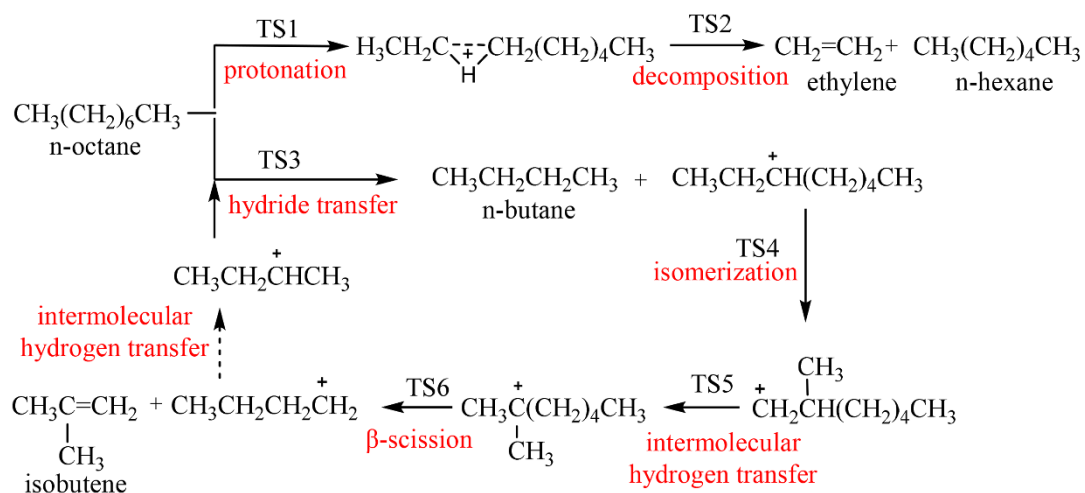


**Figure 2.** Monomolecular and bimolecular cracking pathways of n-octane over zeolites.

175 × 82 mm (1200 × 1200 DPI)

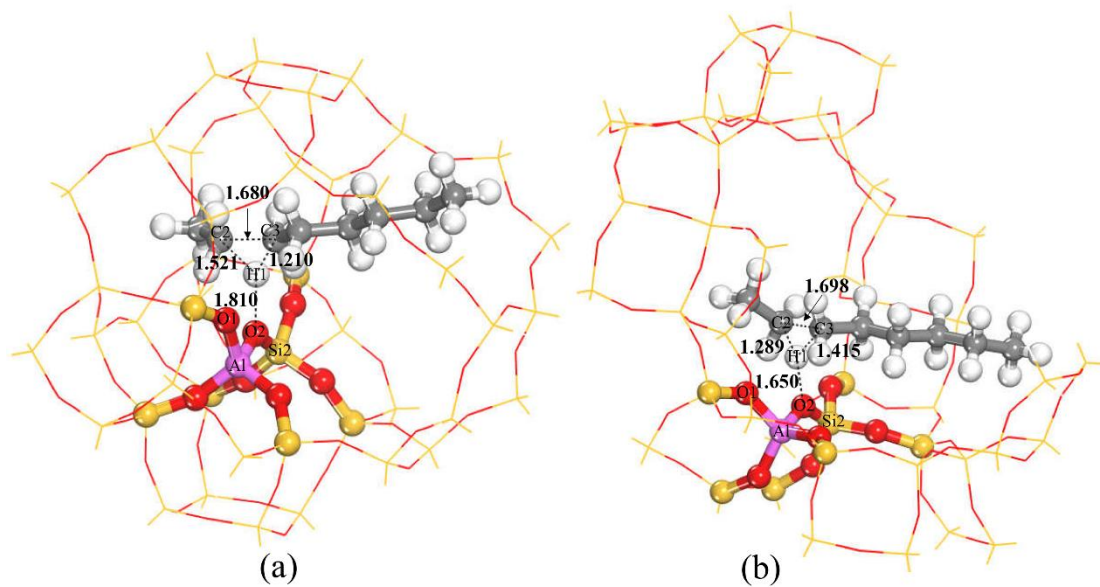


**Figure 3.** Optimized structures of transition states TS1 for protonation reaction of n-octane in the HZSM-5 (a) and HY (b) zeolites.

175×95 mm (600×600 DPI)

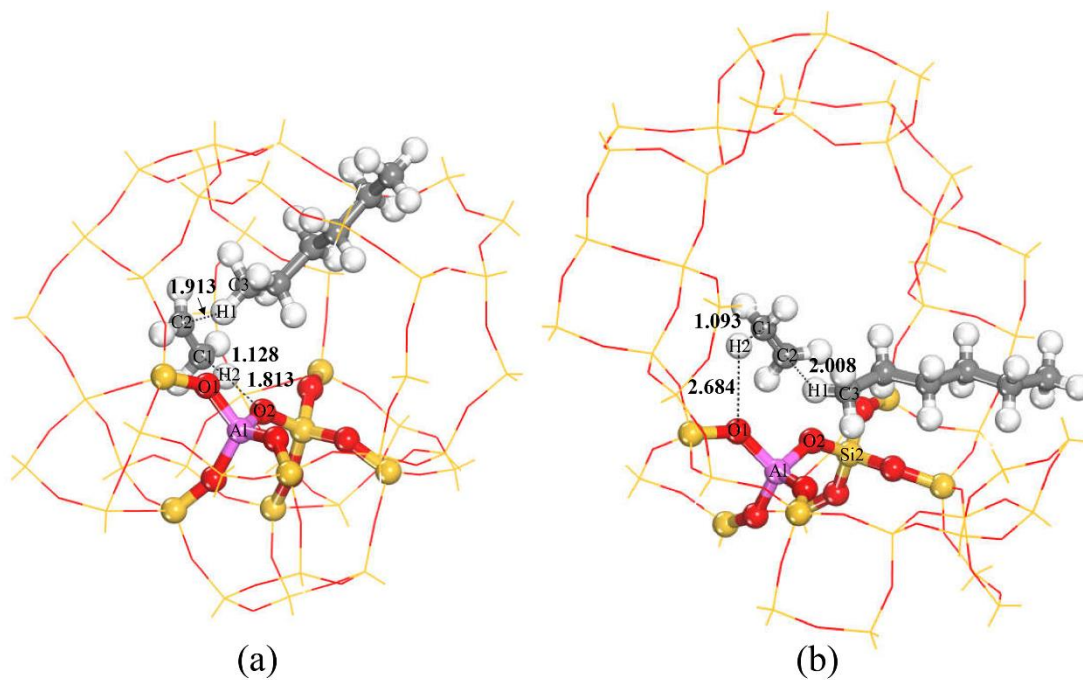


**Figure 4.** Optimized structures of transition states TS2 for decomposition reaction in the HZSM-5 (a) and HY (b) zeolites.

175×100 mm (600×600 DPI)

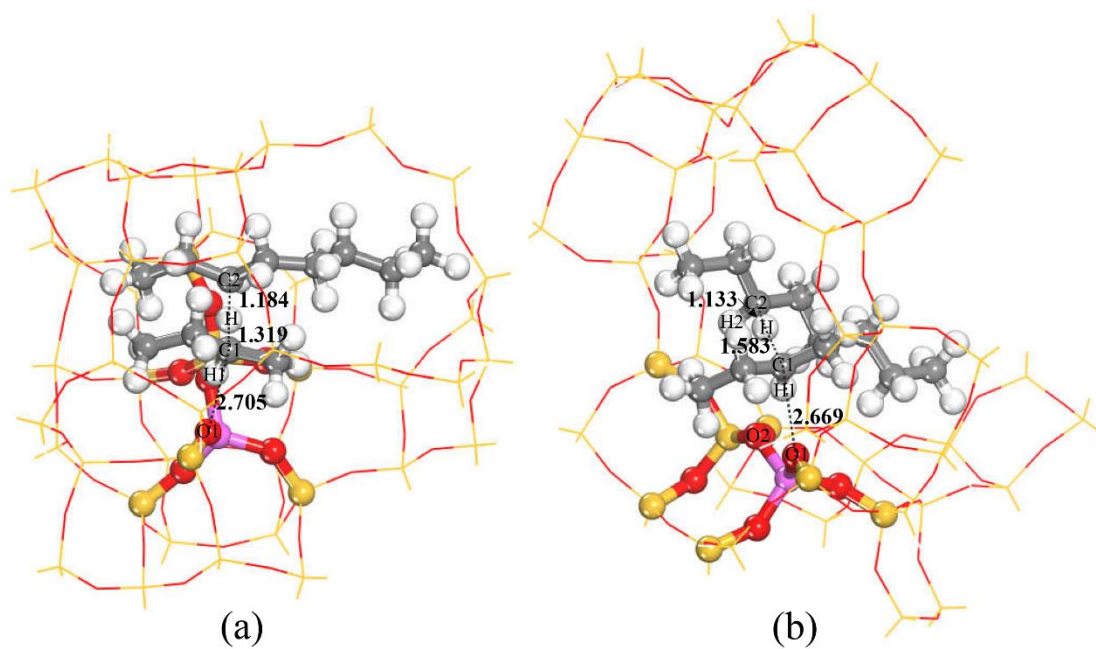


**Figure 5.** Optimized structures of transition states TS3 for hydride transfer reaction in the HZSM-5 (a) and HY (b) zeolites.

175×100 mm (600×600 DPI)

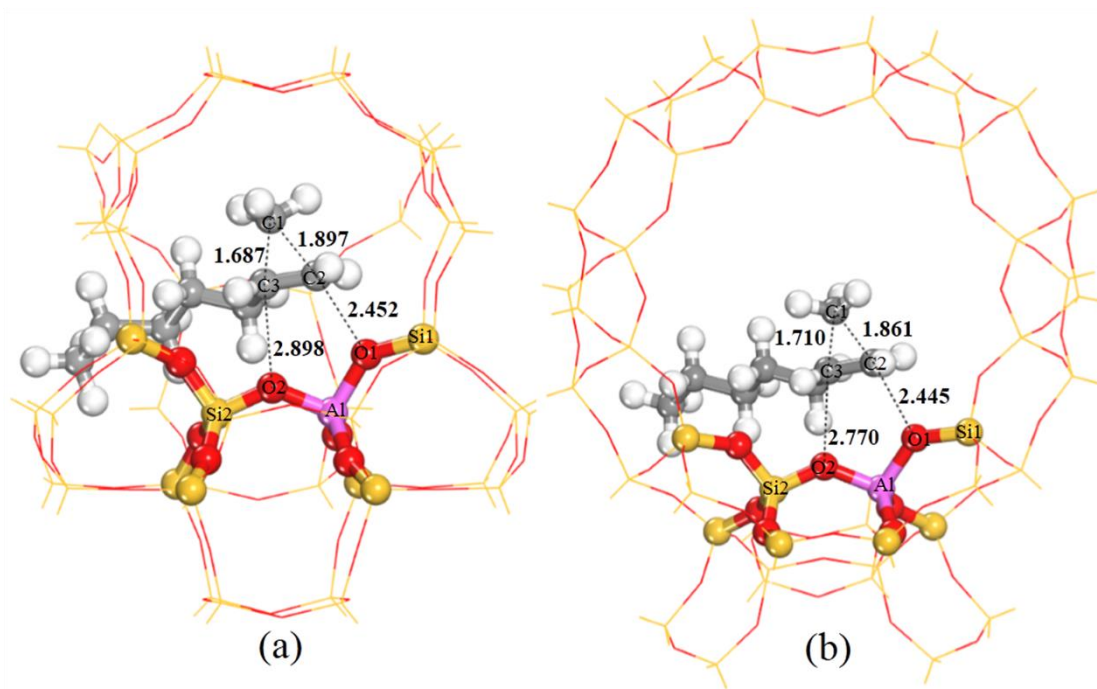


**Figure 6.** Optimized structures of transition states TS4 for isomerization reaction in the HZSM-5 (a) and HY (b) zeolites.

175×108 mm (600×600 DPI)

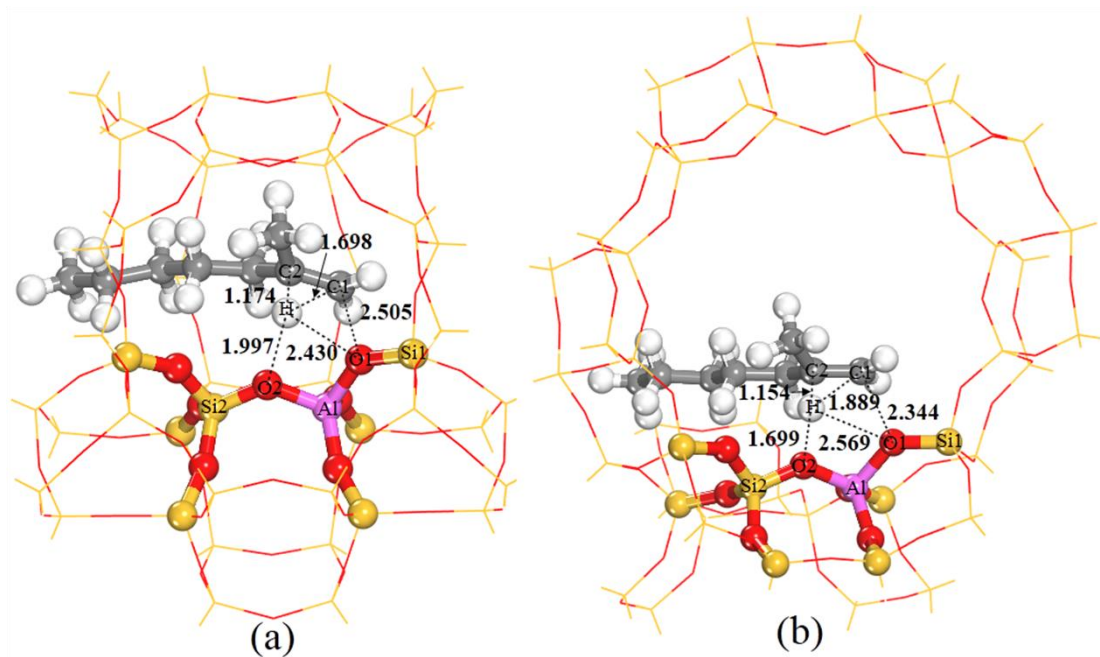


**Figure 7.** Optimized structures of transition states TS5 for intermolecular hydrogen transfer reaction in the HZSM-5 (a) and HY (b) zeolites.

175×104 mm (600×600 DPI)

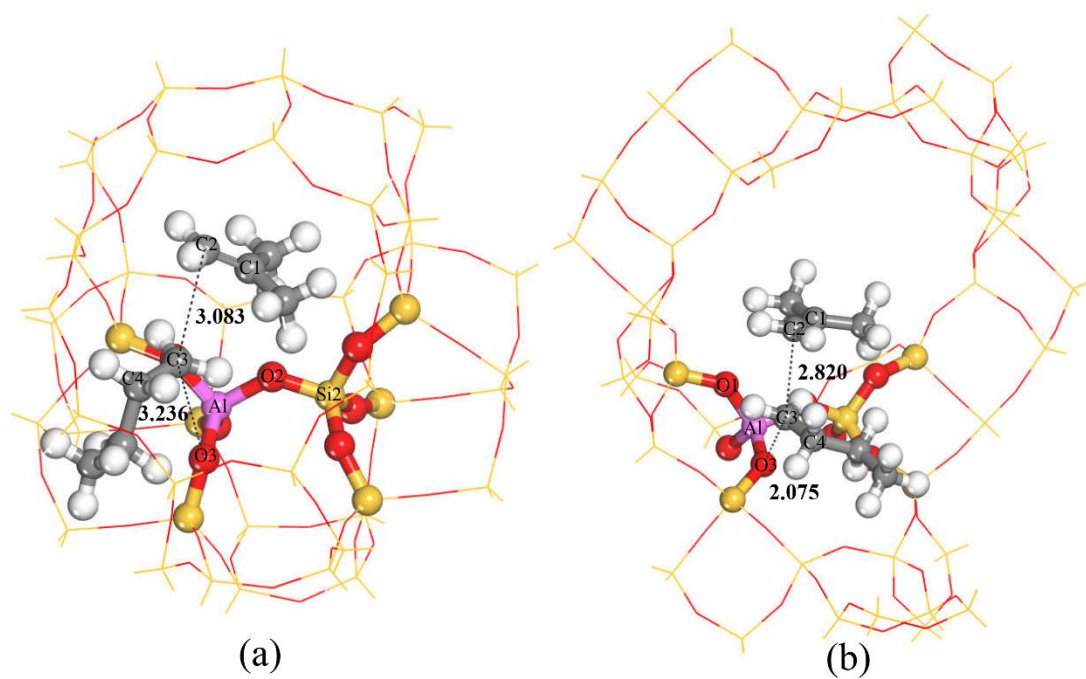


**Figure 8.** Optimized structures of transition states TS6 for the  $\beta$ -scission reaction in the HZSM-5 (a) and HY (b) zeolites.

175×107 mm (600×600 DPI)

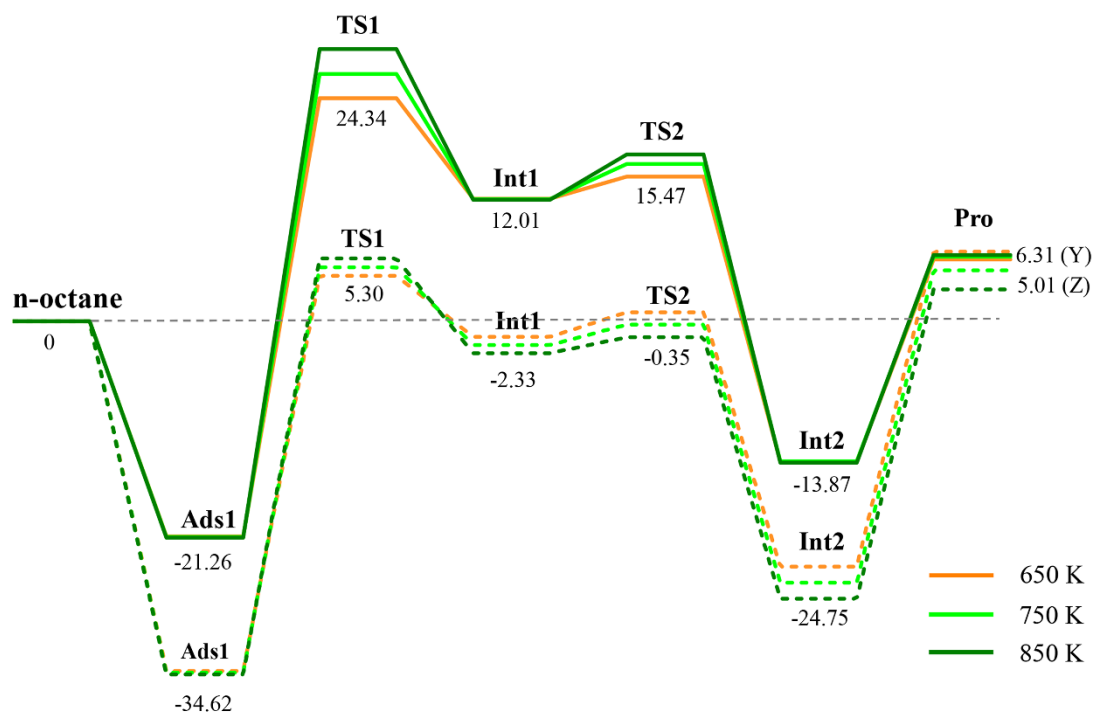


**Figure 9.** The Gibbs free energy for monomolecular cracking mechanism at 650K, 750K and 850K in the HZSM-5 (dash line) and HY (solid line) zeolites. (The energy number labeled at 750K)

175×115 mm (1200×1200 DPI)

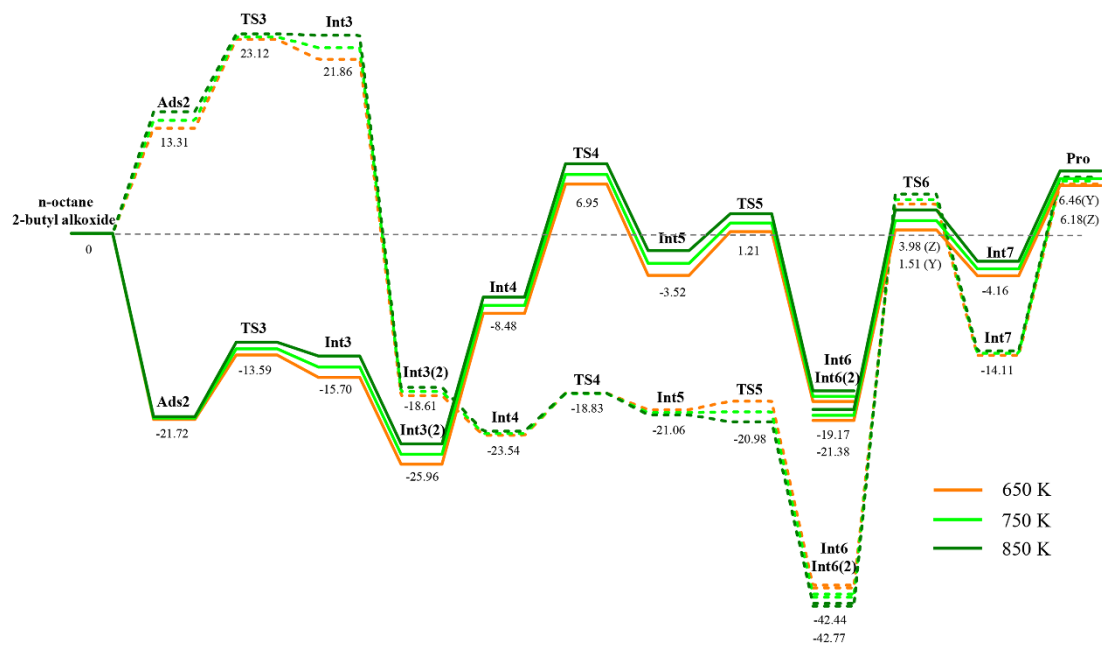


**Figure 10.** The Gibbs free energy for bimolecular cracking mechanism at 650K, 750K and 850K in the HZSM-5 (dash line) and HY (solid line) zeolites. (The energy number labeled at 750K)

175×104 mm (1200×1200 DPI)